

Chapter 5

State point dependence of power exponent

5.1 Analytic expansion of the pressure tensor and energy

Previous work reported in a recent paper [Mar00] discussed the possible analytical dependence of the pressure and energy of liquid argon upon strain rate. Their NEMD simulations modeled liquid argon with accurate two-body and three-body potentials. The pressure was convincingly found to vary as $\dot{\gamma}^2$, at a state point of $(\rho, T) = (1.034 \text{gcm}^{-3}, 135 \text{K})$, which is in liquid phase and is approximately midway between the critical point and the triple point in the argon phase diagram. Further NEMD simulations on liquid xenon [Mar01a] demonstrated even more convincingly the $\dot{\gamma}^2$ dependence of both the pressure and energy. Independent work by Matin, Davis, and Todd [Mat00] suggested that the nonanalytical variation of the energy and pressure as a function of strain rate may be a peculiarity of the triple point, and that an analytical dependence may be observed at other state points.

NEMD simulations of atomic fluids have been overwhelmingly performed at the triple point. This is because simulations performed at higher liquid densities give superior statistical accuracy in all measurable quantities, but also because they have revealed interesting non-analytic functional forms for the phenomenological constitutive relations, agreeing with predictions based on long-time tail theories [Eva80b]. Most work performed at the triple point reports a non-analytical dependence of the energy and pressure on strain rate, in conformity with the predictions of mode coupling theory [Kaw73], i.e.,

$$\begin{aligned} E(\dot{\gamma}) &= E(0) + a\dot{\gamma}^{3/2}, \\ p(\dot{\gamma}) &= p(0) + b\dot{\gamma}^{3/2}. \end{aligned} \tag{5.1}$$

This result is in contrast to what one might expect from expanding the internal energy and pressure tensor as a Taylor series about the thermodynamic driving force, in this case the strain rate tensor, $\nabla \mathbf{u}$. Here \mathbf{u} is the streaming velocity of the fluid. Such an expansion assumes at the outset that both the energy and pressure are analytical functions of the strain rate. If they are not, then no such expansion is possible [Kaw73, Eva90]. For a fluid flowing in the x direction and shearing in the y direction, the strain rate tensor has only one nonzero off-diagonal term,

$$\nabla \mathbf{u} = \begin{pmatrix} \frac{\partial u_x}{\partial x} & \frac{\partial u_y}{\partial x} & \frac{\partial u_z}{\partial x} \\ \frac{\partial u_x}{\partial y} & \frac{\partial u_y}{\partial y} & \frac{\partial u_z}{\partial y} \\ \frac{\partial u_x}{\partial z} & \frac{\partial u_y}{\partial z} & \frac{\partial u_z}{\partial z} \end{pmatrix} = \begin{pmatrix} 0 & 0 & 0 \\ \dot{\gamma} & 0 & 0 \\ 0 & 0 & 0 \end{pmatrix}, \tag{5.2}$$

where $\dot{\gamma} \equiv \partial u_x / \partial y$.

Now consider expanding the total internal energy of the fluid as a function of $\nabla \mathbf{u}$, and truncating at second order:

$$\begin{aligned} E &= E(\nabla \mathbf{u}) \\ &= E(0) + \nabla \mathbf{u} : \left. \frac{\partial E}{\partial (\nabla \mathbf{u})} \right|_{\nabla \mathbf{u}=0} \\ &\quad + \frac{1}{2} (\nabla \mathbf{u})(\nabla \mathbf{u})^{[4]} \left. \frac{\partial^2 E}{\partial (\nabla \mathbf{u}) \partial (\nabla \mathbf{u})} \right|_{\nabla \mathbf{u}=0} + \dots, \end{aligned} \tag{5.3}$$

Here the notation $(\cdot)^{[4]}$ stands for a fourth order contraction between the two fourth rank tensors $(\nabla \mathbf{u})(\nabla \mathbf{u})$ and $[\partial^2 E / \partial(\nabla \mathbf{u})\partial(\nabla \mathbf{u})]_{\nabla \mathbf{u}=0}$.

The two partial derivatives in Eqn. (5.3), $[\partial E / \partial(\nabla \mathbf{u})]_{\nabla \mathbf{u}=0}$ and $[\partial^2 E / \partial(\nabla \mathbf{u})\partial(\nabla \mathbf{u})]_{\nabla \mathbf{u}=0}$, are both evaluated at zero applied thermodynamic force, i.e., at equilibrium. It is reasonable to assume that just as an equilibrium fluid should be isotropic in space, so too should be the phenomenological coefficient tensors that are descriptive of their material properties. This allows their form to be simplified. As the first order partial derivative is a second rank isotropic tensor, it can be expressed as

$$\left. \frac{\partial E}{\partial(\nabla \mathbf{u})} \right|_{\nabla \mathbf{u}=0} = a \delta_{\alpha\beta} \quad (5.4)$$

where a is constant. Therefore, the second term in Eqn. (5.3) can be written as

$$E^{(2)} \equiv \nabla \mathbf{u} : \left. \frac{\partial E}{\partial(\nabla \mathbf{u})} \right|_{\nabla \mathbf{u}=0} = \nabla_{\beta} u_{\alpha} a \delta_{\alpha\beta} = a \nabla_{\beta} u_{\beta} = 0. \quad (5.5)$$

In the above derivation and subsequent derivations, the Einstein notation for contraction of tensor indices is used.

The second order partial derivative in Eqn. (5.3) is a fourth rank isotropic tensor, which may be expanded as a linear combination of the three isotropic fourth rank polar tensors [Eva90, Dai93, Spi74]:

$$\begin{aligned} \left. \frac{\partial^2 E}{\partial(\nabla \mathbf{u})\partial(\nabla \mathbf{u})} \right|_{\nabla \mathbf{u}=0} &\equiv B_{\alpha\beta\gamma\delta} \\ &= b_1 \delta_{\alpha\beta} \delta_{\gamma\delta} + b_2 \delta_{\alpha\gamma} \delta_{\beta\delta} + b_3 \delta_{\alpha\delta} \delta_{\gamma\beta}. \end{aligned} \quad (5.6)$$

Therefore the third term in Eqn. (5.3) can be written as

$$\begin{aligned}
E^{(3)} &\equiv \frac{1}{2}(\nabla \mathbf{u})(\nabla \mathbf{u})(\cdot)^{[4]} \frac{\partial^2 E}{\partial(\nabla \mathbf{u})\partial(\nabla \mathbf{u})} \Big|_{\nabla \mathbf{u}=0} \\
&= \frac{1}{2}(\nabla_{\delta} u_{\gamma})(\nabla_{\beta} u_{\alpha}) B_{\alpha\beta\gamma\delta}.
\end{aligned} \tag{5.7}$$

Substituting Eqn. (5.6) into Eqn. (5.7), one finds

$$E^{(3)} = \frac{1}{2} b_2 \dot{\gamma}^2. \tag{5.8}$$

Finally, substituting Eqn. (5.5) and (5.8) into Eqn. (5.3) gives

$$E(\dot{\gamma}) = E(0) + \frac{1}{2} b_2 \dot{\gamma}^2. \tag{5.9}$$

In a similar way, we may expand the pressure tensor as a function of powers of the strain rate tensor, and truncate at second order:

$$\begin{aligned}
\mathbf{P} = \mathbf{P}(\nabla \mathbf{u}) &= \mathbf{P}(0) + \nabla \mathbf{u} : \frac{\partial \mathbf{P}}{\partial(\nabla \mathbf{u})} \Big|_{\nabla \mathbf{u}=0} \\
&+ \frac{1}{2}(\nabla \mathbf{u})(\nabla \mathbf{u})(\cdot)^{[4]} \frac{\partial^2 \mathbf{P}}{\partial(\nabla \mathbf{u})\partial(\nabla \mathbf{u})} \Big|_{\nabla \mathbf{u}=0} + \dots \\
&= p_0 \mathbf{1} + \nabla \mathbf{u} : \frac{\partial \mathbf{P}}{\partial(\nabla \mathbf{u})} \Big|_{\nabla \mathbf{u}=0} + \frac{1}{2}(\nabla \mathbf{u})(\nabla \mathbf{u}) \\
&\quad \times (\cdot)^{[4]} \frac{\partial^2 \mathbf{P}}{\partial(\nabla \mathbf{u})\partial(\nabla \mathbf{u})} \Big|_{\nabla \mathbf{u}=0} + \dots,
\end{aligned} \tag{5.10}$$

Here the unit tensor is defined as $\mathbf{1}$, and the equilibrium isotropic pressure is designated as p_0 . Now the second term involves a second order contraction of a second rank tensor $(\nabla \mathbf{u})$, with a fourth rank tensor, $[\partial \mathbf{P} / \partial(\nabla \mathbf{u})]_{\nabla \mathbf{u}=0}$. Similarly, the third term represents a fourth order

contraction of a fourth rank tensor $(\nabla \mathbf{u})(\nabla \mathbf{u})$ with a sixth rank tensor, $[\partial^2 \mathbf{P} / \partial(\nabla \mathbf{u}) \partial(\nabla \mathbf{u})]_{\nabla \mathbf{u}=0}$. Both contractions result in second rank tensors, as required.

Defining the non-equilibrium part of the total pressure as $\mathbf{\Pi} \equiv \mathbf{P} - p_0 \mathbf{1}$, we have

$$\begin{aligned} \mathbf{\Pi} &= \nabla \mathbf{u} : \left. \frac{\partial \mathbf{P}}{\partial(\nabla \mathbf{u})} \right|_{\nabla \mathbf{u}=0} \\ &+ \frac{1}{2} (\nabla \mathbf{u})(\nabla \mathbf{u})(\cdot)^{[4]} \left. \frac{\partial^2 \mathbf{P}}{\partial(\nabla \mathbf{u}) \partial(\nabla \mathbf{u})} \right|_{\nabla \mathbf{u}=0} + \dots \\ &\equiv \mathbf{\Pi}^{(1)} + \mathbf{\Pi}^{(2)} + \dots. \end{aligned} \quad (5.11)$$

The first order partial derivative is a fourth order isotropic tensor, expressible as a linear combination of the three isotropic fourth rank polar tensors as before:

$$\left. \frac{\partial \mathbf{P}}{\partial(\nabla \mathbf{u})} \right|_{\nabla \mathbf{u}=0} \equiv B_{\alpha\beta\gamma\delta} = b_1 \delta_{\alpha\beta} \delta_{\gamma\delta} + b_2 \delta_{\alpha\gamma} \delta_{\beta\delta} + b_3 \delta_{\alpha\delta} \delta_{\gamma\beta}, \quad (5.12)$$

where b_1 , b_2 and b_3 are constants.

Substituting Eqn. (5.12) into Eqn. (5.11), and performing the necessary algebra, leads to the following simplification for the first term:

$$\mathbf{\Pi}^{(1)} = \dot{\gamma} \begin{pmatrix} 0 & b_2 & 0 \\ b_3 & 0 & 0 \\ 0 & 0 & 0 \end{pmatrix}. \quad (5.13)$$

The second order partial derivative in Eqn. (5.11) is a sixth rank isotropic tensor, so it may be expressed as a linear combination of the 15 independent isotropic sixth rank tensors:

$$\begin{aligned}
\left. \frac{\partial^2 \mathbf{P}}{\partial(\nabla \mathbf{u}) \partial(\nabla \mathbf{u})} \right|_{\nabla \mathbf{u}=0} &\equiv E_{\alpha\beta\gamma\delta\epsilon\zeta} \\
&= e_1 \delta_{\alpha\beta} \delta_{\gamma\epsilon} \delta_{\delta\zeta} + e_2 \delta_{\alpha\beta} \delta_{\gamma\delta} \delta_{\epsilon\zeta} + e_3 \delta_{\alpha\beta} \delta_{\gamma\zeta} \delta_{\delta\epsilon} + e_4 \delta_{\alpha\gamma} \delta_{\beta\delta} \delta_{\epsilon\zeta} + e_5 \delta_{\alpha\gamma} \delta_{\beta\epsilon} \delta_{\delta\zeta} \\
&+ e_6 \delta_{\alpha\gamma} \delta_{\beta\zeta} \delta_{\epsilon\delta} + e_7 \delta_{\alpha\delta} \delta_{\beta\gamma} \delta_{\epsilon\zeta} + e_8 \delta_{\alpha\delta} \delta_{\beta\epsilon} \delta_{\gamma\zeta} + e_9 \delta_{\alpha\delta} \delta_{\beta\zeta} \delta_{\epsilon\gamma} + e_{10} \delta_{\alpha\epsilon} \delta_{\gamma\delta} \delta_{\beta\zeta} \\
&+ e_{11} \delta_{\alpha\epsilon} \delta_{\beta\gamma} \delta_{\delta\zeta} + e_{12} \delta_{\alpha\epsilon} \delta_{\gamma\zeta} \delta_{\beta\delta} + e_{13} \delta_{\alpha\zeta} \delta_{\gamma\delta} \delta_{\epsilon\beta} + e_{14} \delta_{\alpha\zeta} \delta_{\beta\gamma} \delta_{\delta\epsilon} + e_{15} \delta_{\alpha\zeta} \delta_{\gamma\epsilon} \delta_{\beta\delta}.
\end{aligned} \tag{5.14}$$

where $e_1, e_2, e_3, \dots, e_{15}$ are all constants.

Substituting Eqn. (5.14) into Eqn. (5.11), and performing the required manipulations, leads to

$$\mathbf{\Pi}^{(2)} = \frac{1}{2} \dot{\gamma}^2 \begin{pmatrix} e_4 + e_{12} + e_{15} & 0 & 0 \\ 0 & e_4 + e_5 + e_6 & 0 \\ 0 & 0 & e_4 \end{pmatrix}. \tag{5.15}$$

Substituting Eqn. (5.13) and (5.15) into Eqn. (5.11) gives

$$\begin{aligned}
\mathbf{\Pi} &= \dot{\gamma} \begin{pmatrix} 0 & b_2 & 0 \\ b_3 & 0 & 0 \\ 0 & 0 & 0 \end{pmatrix} \\
&+ \frac{1}{2} \dot{\gamma}^2 \begin{pmatrix} e_4 + e_{12} + e_{15} & 0 & 0 \\ 0 & e_4 + e_5 + e_6 & 0 \\ 0 & 0 & e_4 \end{pmatrix}.
\end{aligned} \tag{5.16}$$

The isotropic pressure is determined as

$$\begin{aligned}
p(\dot{\gamma}) &\equiv \frac{1}{3} \mathbf{Tr}(\mathbf{P}) \\
&= p_0 + \frac{1}{3} \mathbf{Tr}(\mathbf{\Pi}) \\
&= p_0 + \frac{1}{6} [3e_4 + e_5 + e_6 + e_{12} + e_{15}] \dot{\gamma}^2.
\end{aligned} \tag{5.17}$$

Equations (5.9) and (5.17) show that if the energy and pressure are analytic in powers of the strain rate, then their leading terms must be $\dot{\gamma}^2$. While there are terms involving $\dot{\gamma}$ in the pressure tensor expansion, they are off-diagonal terms related to the shear stress. In fact, the constants b_2 and b_3 are equivalent, and equal in magnitude to the shear viscosity η . Only diagonal terms contribute to the isotropic pressure.

5.2 Simulation at three state points

To check the dependence of pressure and energy on strain rate, we performed nonequilibrium molecular dynamics simulations. Our simulations were conducted on a Lennard-Jones fluid of 500 atoms at three distinct state points: the Lennard-Jones triple point $(T, \rho) = (0.722, 0.8442)$; a point midway between the triple point and the critical point, $(T, \rho) = (0.97, 0.61)$; and a high point close to the critical temperature, $(T, \rho) = (1.1, 0.643)$. The normal convention was adopted for the reduced density ($\rho^* = \rho\sigma^3$), temperature ($T^* = kT/\varepsilon$), energy ($E^* = E/\varepsilon$), pressure ($p^* = p\sigma^3/\varepsilon$), strain rate ($\dot{\gamma}^* = [\sigma(m/\varepsilon)^{1/2}]\dot{\gamma}$), and time ($\tau^* = [\varepsilon/m\sigma^2]^{1/2}\tau$). All quantities quoted in this work are in terms of these reduced quantities and the superscript asterisk will be omitted. The Lennard-Jones potential was used (see Eqn. (4.5)). The parameters ε and σ were set at 1, and a cutoff radius of half the box length was chosen.

The NEMD simulations were performed by applying the SLLD equations of motion for planar shear flow as described in Chapter 4.7. A Gaussian thermostat was used to keep the kinetic temperature of the fluid constant. The equations of motion were integrated with a fourth order Gear predictor-corrector scheme [Gea71], with a reduced integration time step of 0.001. A nonequilibrium simulation trajectory is typically run for 200 000 time steps. Averages are taken over 4-5 independent trajectories, each starting at a new configuration. To equilibrate the system, each trajectory is first run without a shearing field. After the shearing field is switched on, the first 50 000 time steps of each trajectory are ignored, and the fluid is allowed to relax to a nonequilibrium steady state. Therefore every pressure and

energy data point represents a total run length of $(4-5) \times 200000 = 8 \times 10^5 - 1 \times 10^6$ time steps.

In Figures 5.1 to 5.4 we plot the pressure and potential energy per particle of the fluid at the Lennard-Jones triple point as functions of $\dot{\gamma}^{3/2}$ and $\dot{\gamma}^2$. As expected, the energy and pressure appear to be linear in $\dot{\gamma}^{3/2}$, though a close examination does suggest a slight systematic deviation from linearity. A plot of the pressure and energy as functions of $\dot{\gamma}^2$ gives very poor fits to the data.

We can use a quantity called the average absolute deviation (AAD) [Sad95] to qualify the goodness of the fitting function:

$$\text{AAD} = \frac{1}{N} \sum_{i=1}^N \left| \frac{d_{sim} - d_{fit}}{d_{sim}} \right| \quad (5.18)$$

where N is the number of data points, d_{sim} is the data from simulation, d_{fit} is the data from fitting. The lower the value of the AAD(%), the more faithfully the curve fits the simulation data.

A comparison of the average absolute deviations (AAD) for both pressure and energy curves at the triple point demonstrates a 2-3-fold improvement in the quality of the agreement between the data for the $\dot{\gamma}^{3/2}$ fit compared to the $\dot{\gamma}^2$ fit.

In Figures 5.5 to 5.8, we plot the pressure and energy of the fluid at the ‘mid-point’ as functions of $\dot{\gamma}^{3/2}$ and $\dot{\gamma}^2$, respectively. In this case both the pressure and energy show systematic departures from linearity when plotted against $\dot{\gamma}^{3/2}$. However, when plotted against $\dot{\gamma}^2$ the fits are excellent. A comparison of the AAD’s for both fits now shows that the $\dot{\gamma}^2$ curves give an almost fourfold improvement over those for $\dot{\gamma}^{3/2}$, reversing the behavior at the triple point. A similar result is also seen for the ‘high point’ data in Figures

5.9 to 5.12. We make no comparisons on the viscosity data at this stage, but will present viscosity data at the end of this chapter.

Our simulation results show a clear departure from the expected $\dot{\gamma}^{3/2}$ dependence of pressure and energy on strain rate away from the triple point. This result should be true irrespective of the type of intermolecular potential used [Kaw73], and is consistent with the suggestion made by Matin, Daivis, and Todd [Mat00] that the $\dot{\gamma}^{3/2}$ dependence may be a peculiarity of fluids close to the triple point. Our simulations away from the triple point were suggestive of an analytic dependence of pressure and energy on the strain rate, the leading term being $\dot{\gamma}^2$, as demonstrated by a Taylor series expansion of both quantities. While our simulations confirm the leading term in these expansions, a deeper understanding of why such a discrepancy exists between the triple point and other state points remains elusive at this stage.

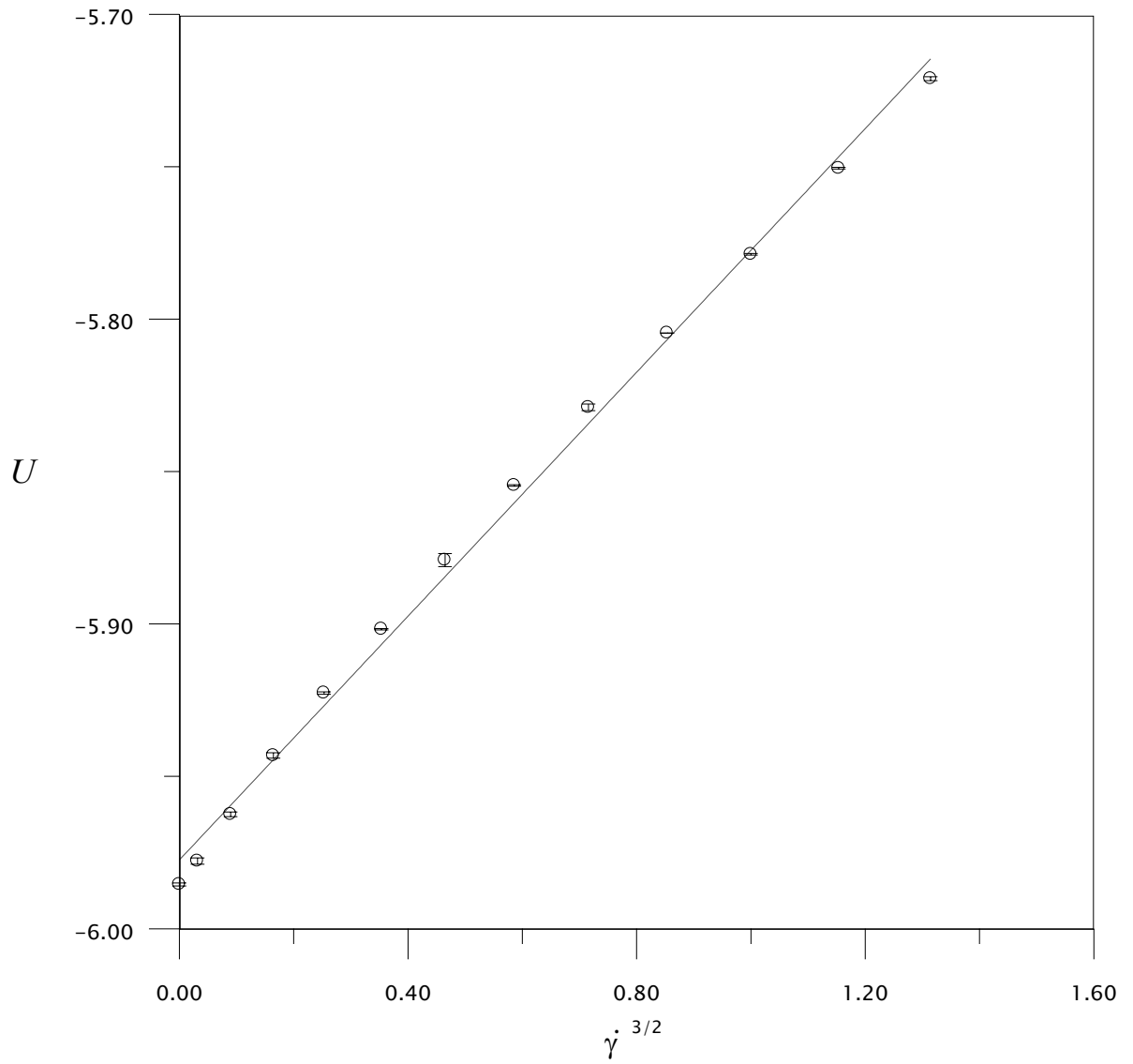


Figure 5.1 Potential energy per atom as a function of $\dot{\gamma}^{3/2}$ at triple point.

The solid line shows a linear fit with an AAD of 0.11%.

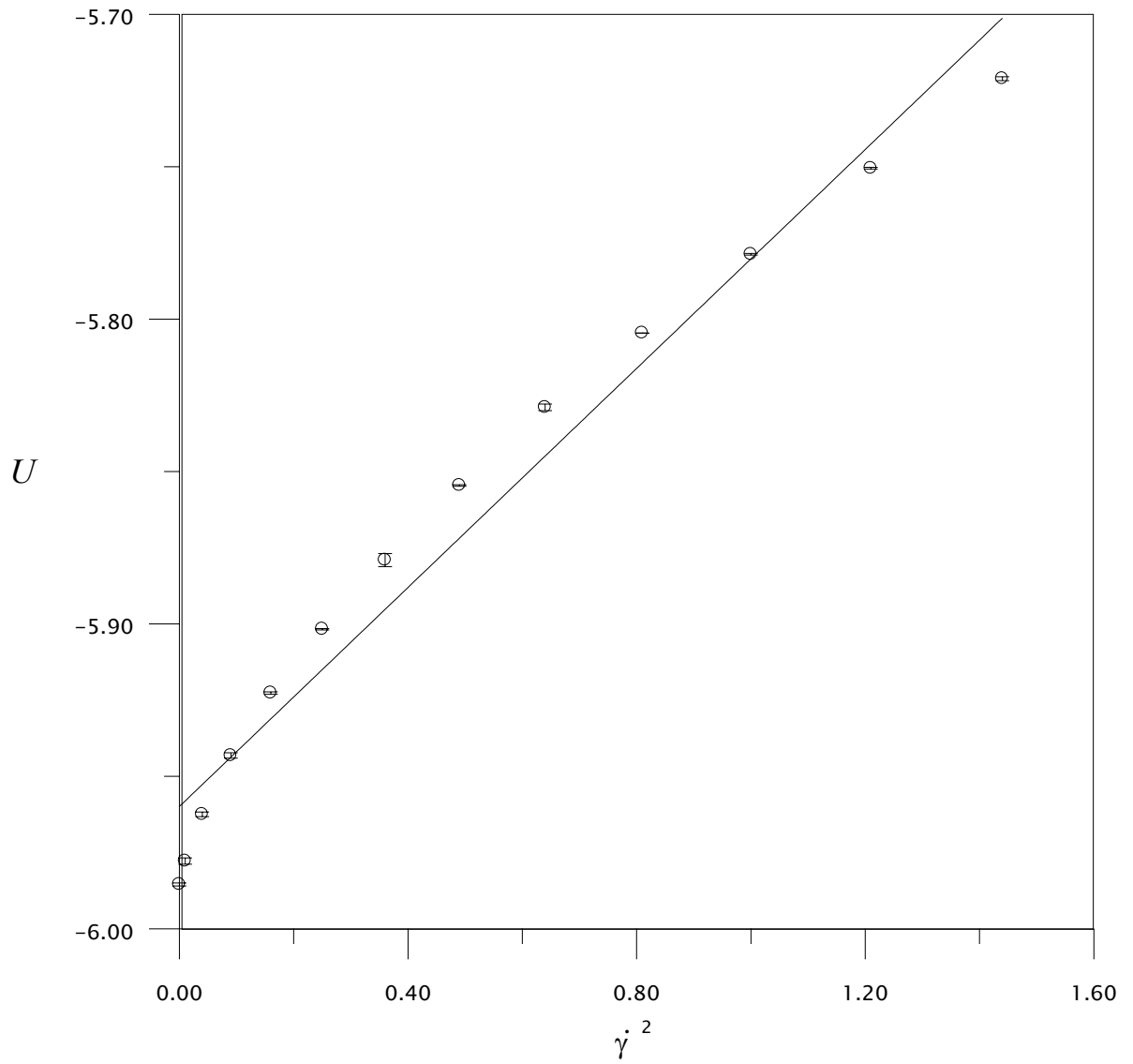


Figure 5.2 Potential energy per atom as a function of $\dot{\gamma}^2$ at triple point.

The solid line shows a linear fit with an AAD of 0.30%.

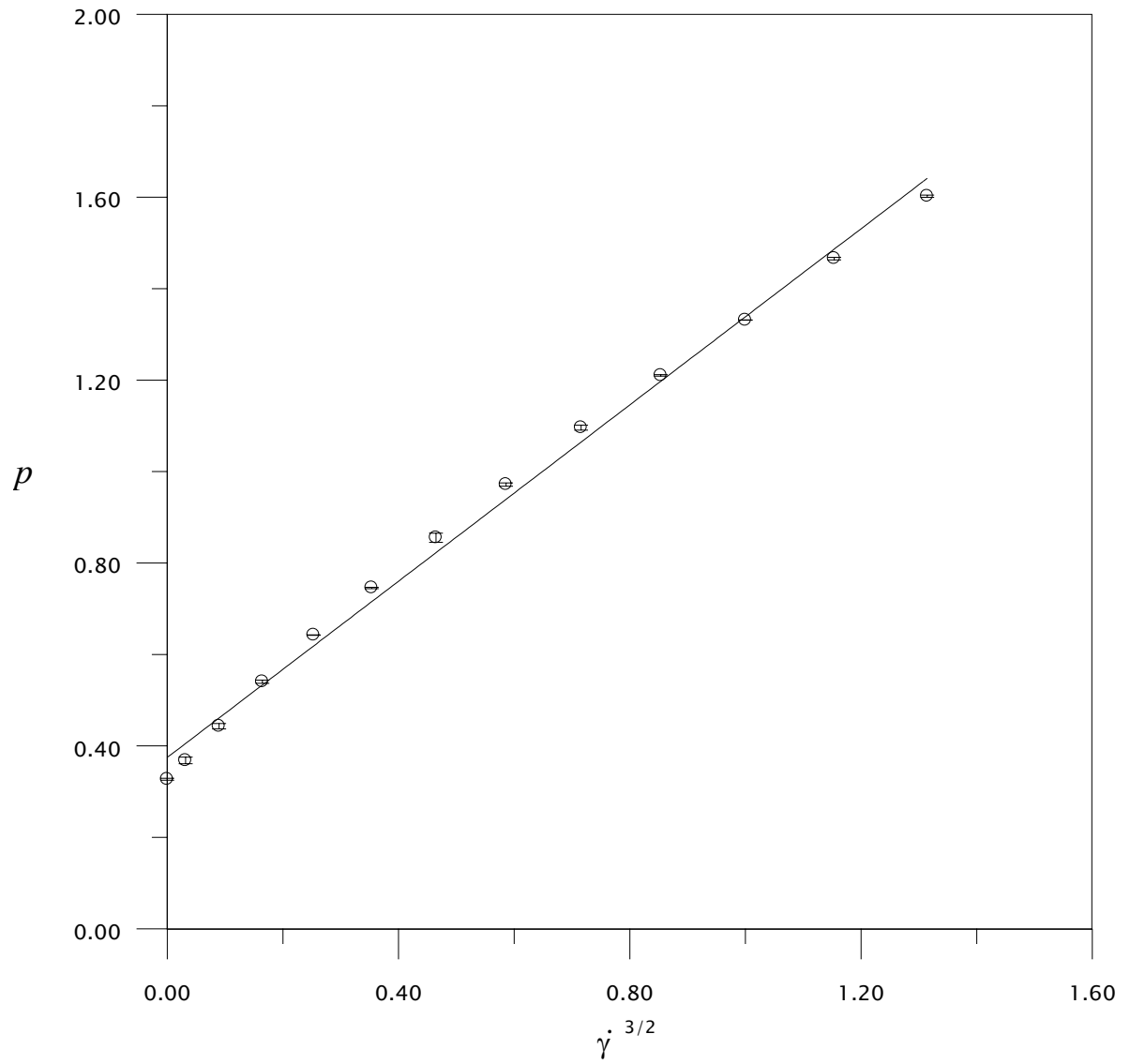


Figure 5.3 Pressure as a function of $\dot{\gamma}^{3/2}$ at triple point.
The solid line shows a linear fit with an AAD of 1.55%.

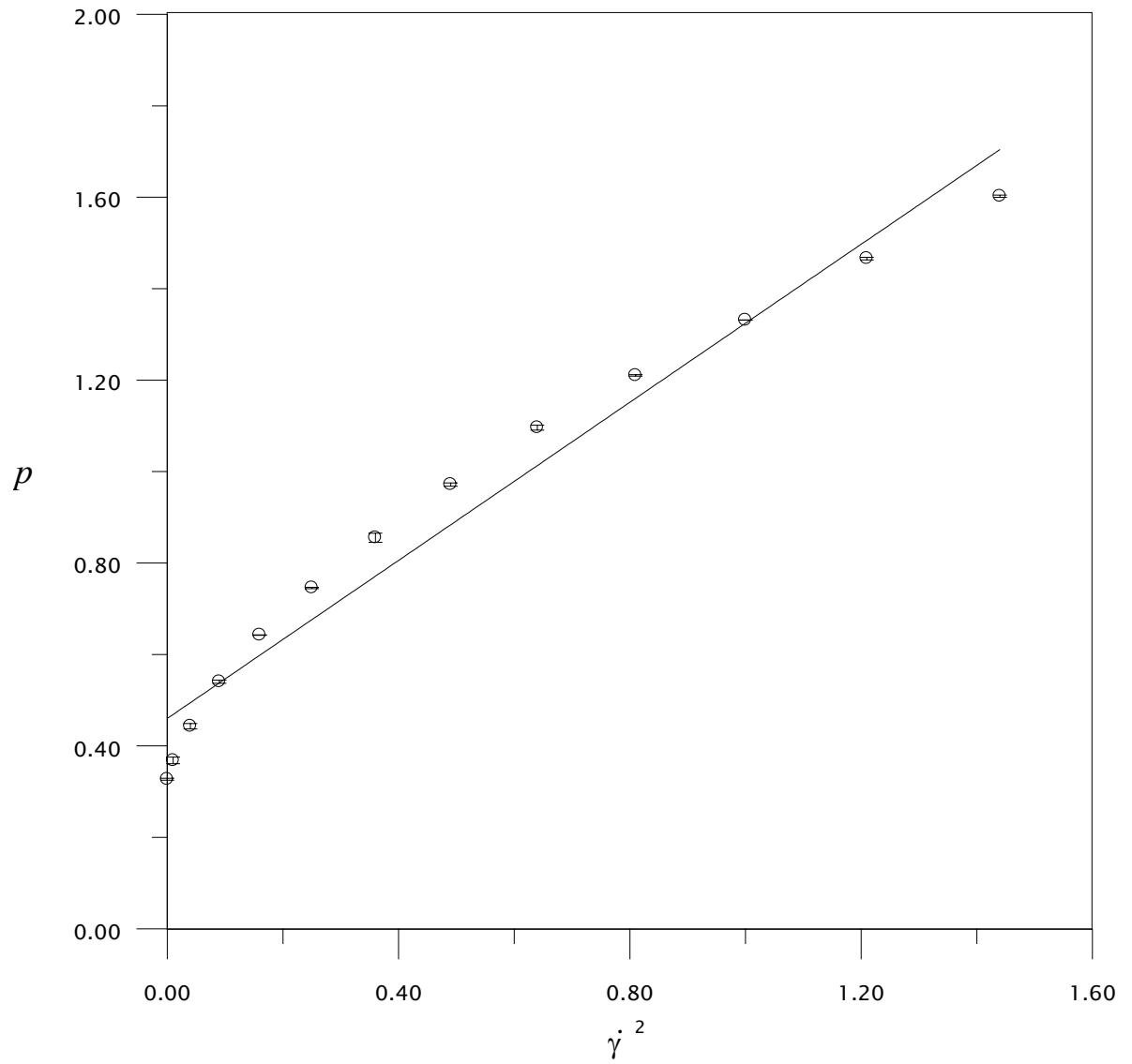


Figure 5.4 Pressure as a function of $\dot{\gamma}^2$ at triple point.
The solid line shows a linear fit with an AAD of 3.78%.

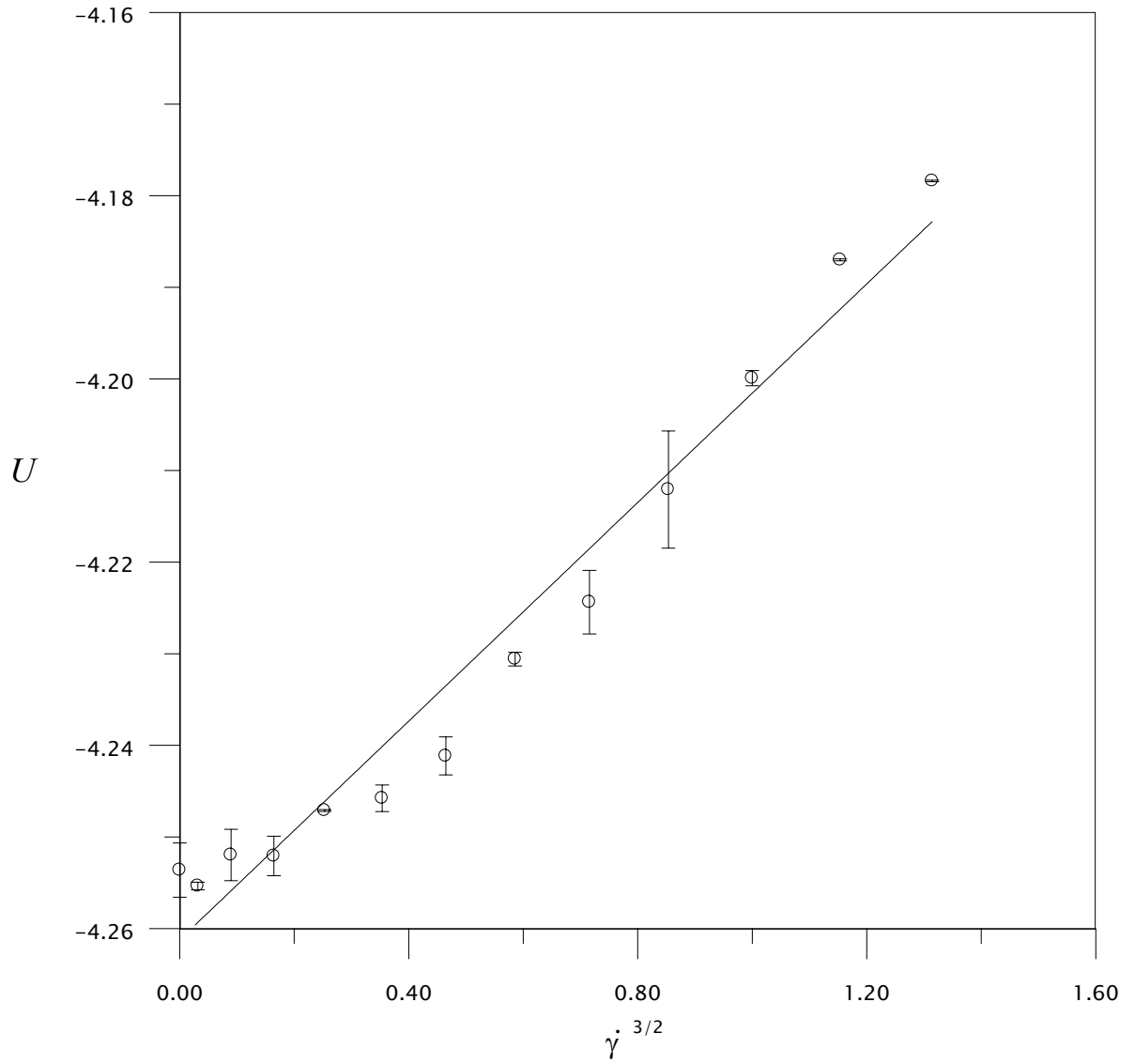


Figure 5.5 Potential energy per atom as a function of $\dot{\gamma}^{3/2}$ at middle point.

The solid line shows a linear fit with an AAD of 0.05%.

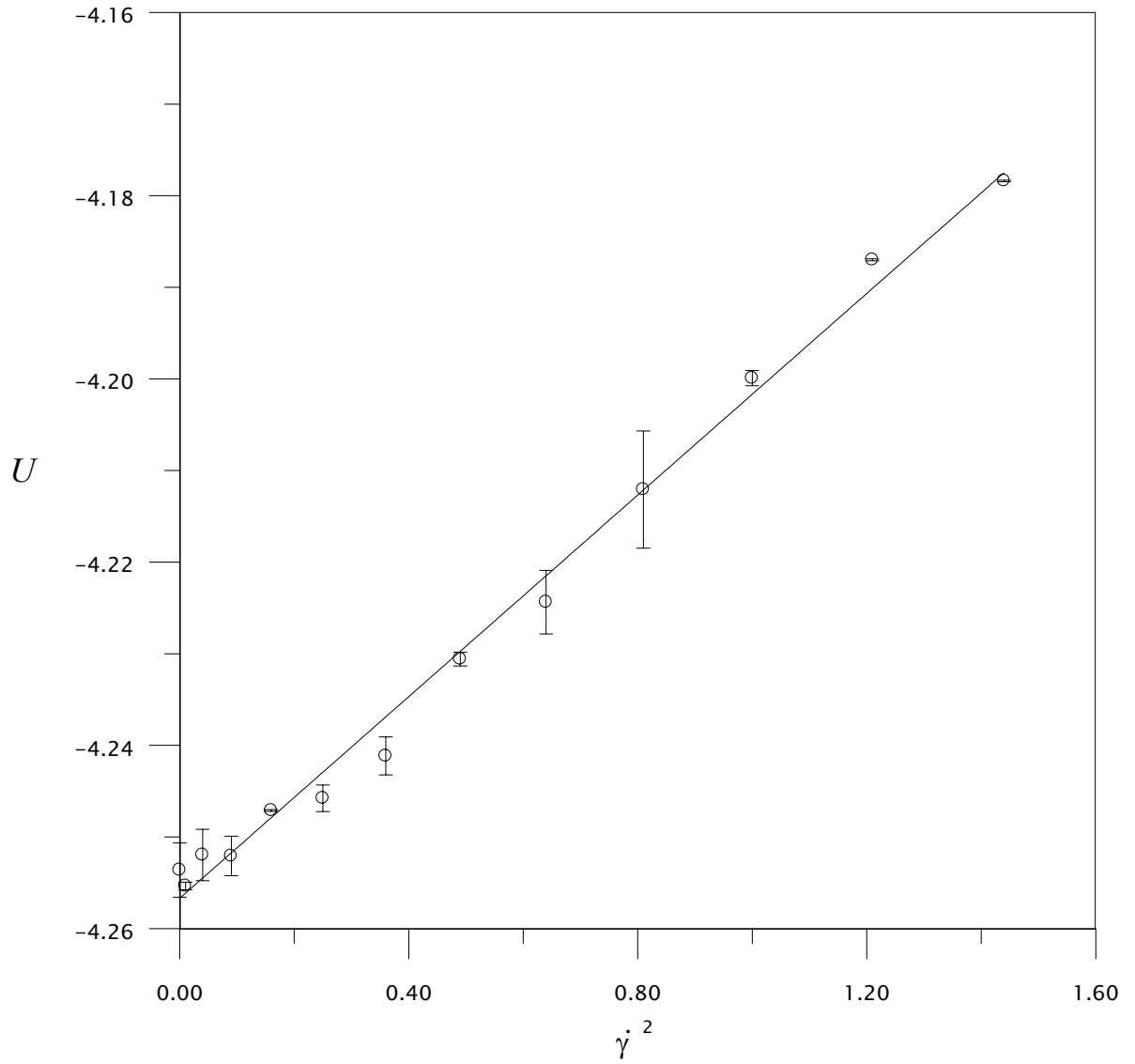


Figure 5.6 Potential energy per atom as a function of $\dot{\gamma}^2$ at middle point.

The solid line shows a linear fit with an AAD of 0.02%.

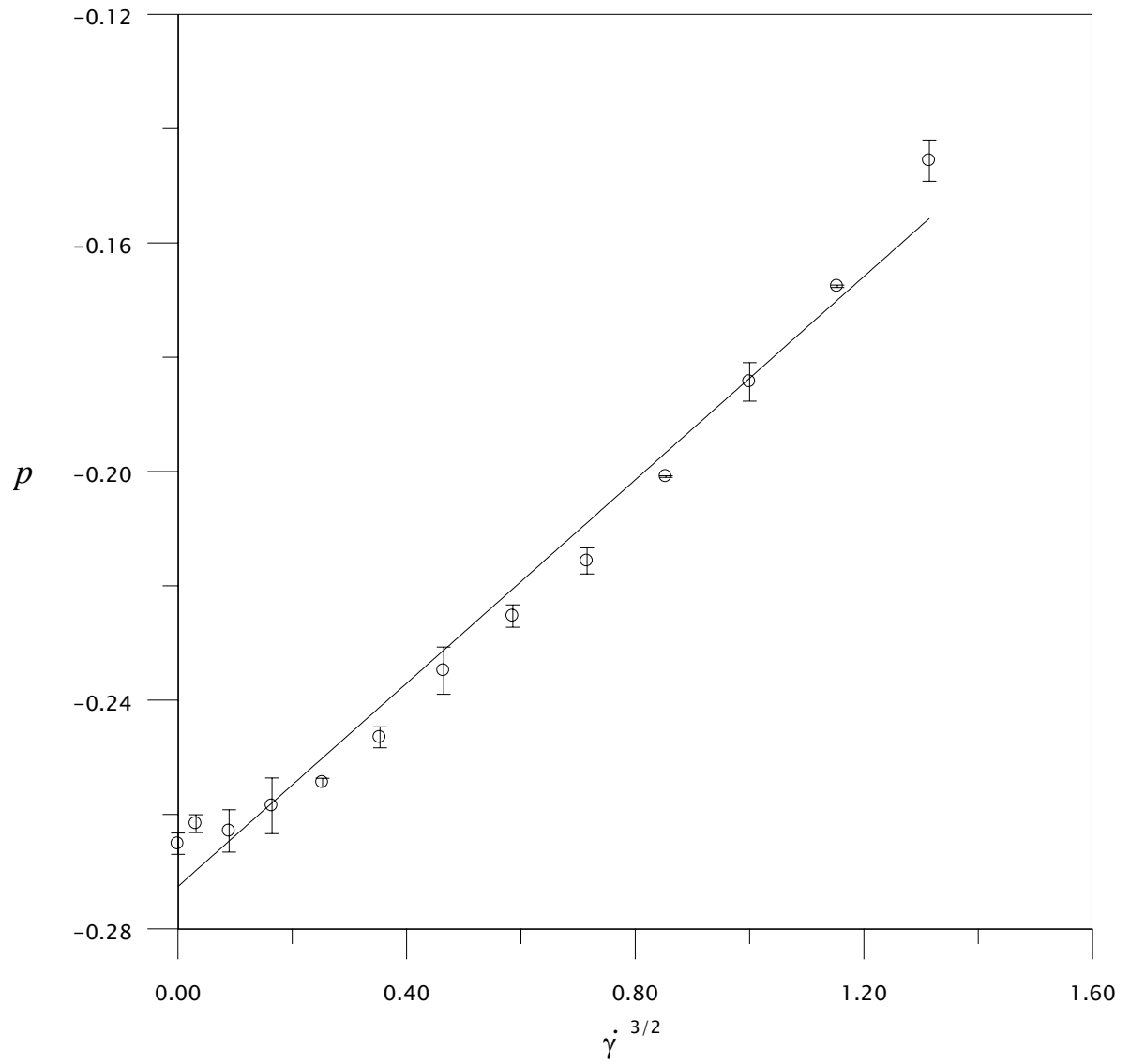


Figure 5.7 Pressure as a function of $\dot{\gamma}^{3/2}$ at middle point.
The solid line shows a linear fit with an AAD of 2.81%.

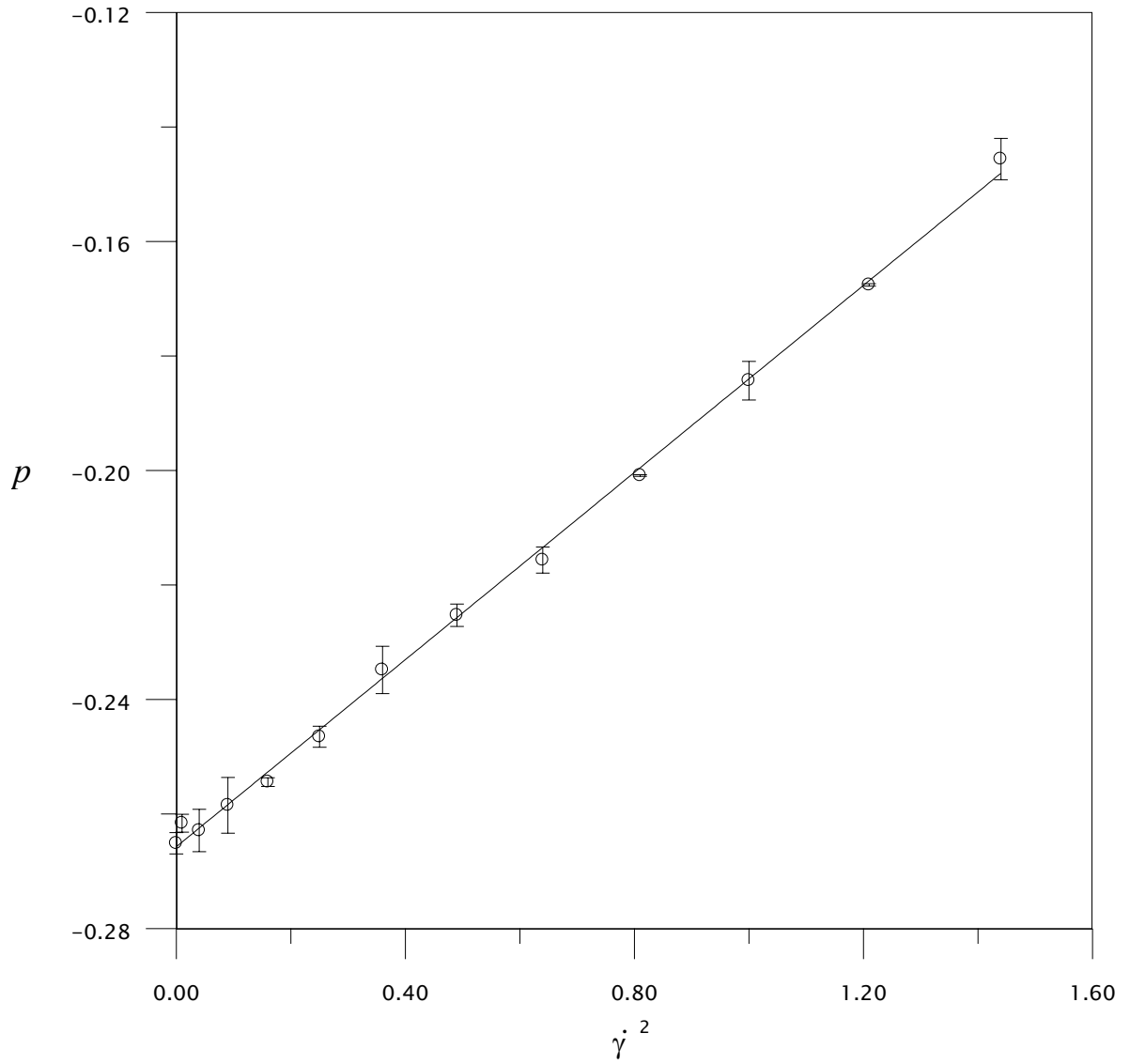


Figure 5.8 Pressure as a function of $\dot{\gamma}^2$ at middle point.
The solid line shows a linear fit with an AAD of 0.76%.

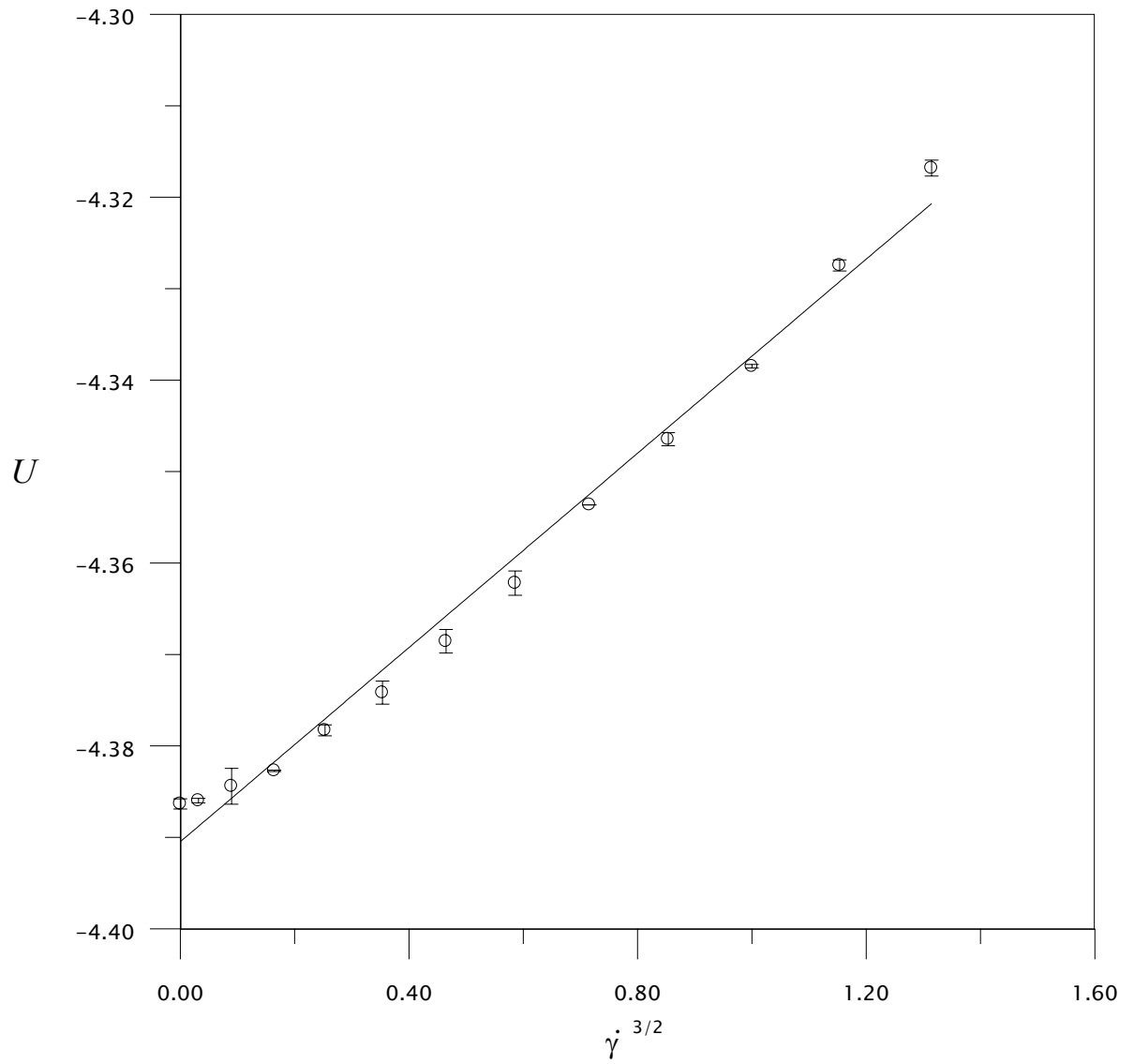


Figure 5.9 Potential energy per atom as a function of $\dot{\gamma}^{3/2}$ at high point.

The solid line shows a linear fit with an AAD of 0.05%.

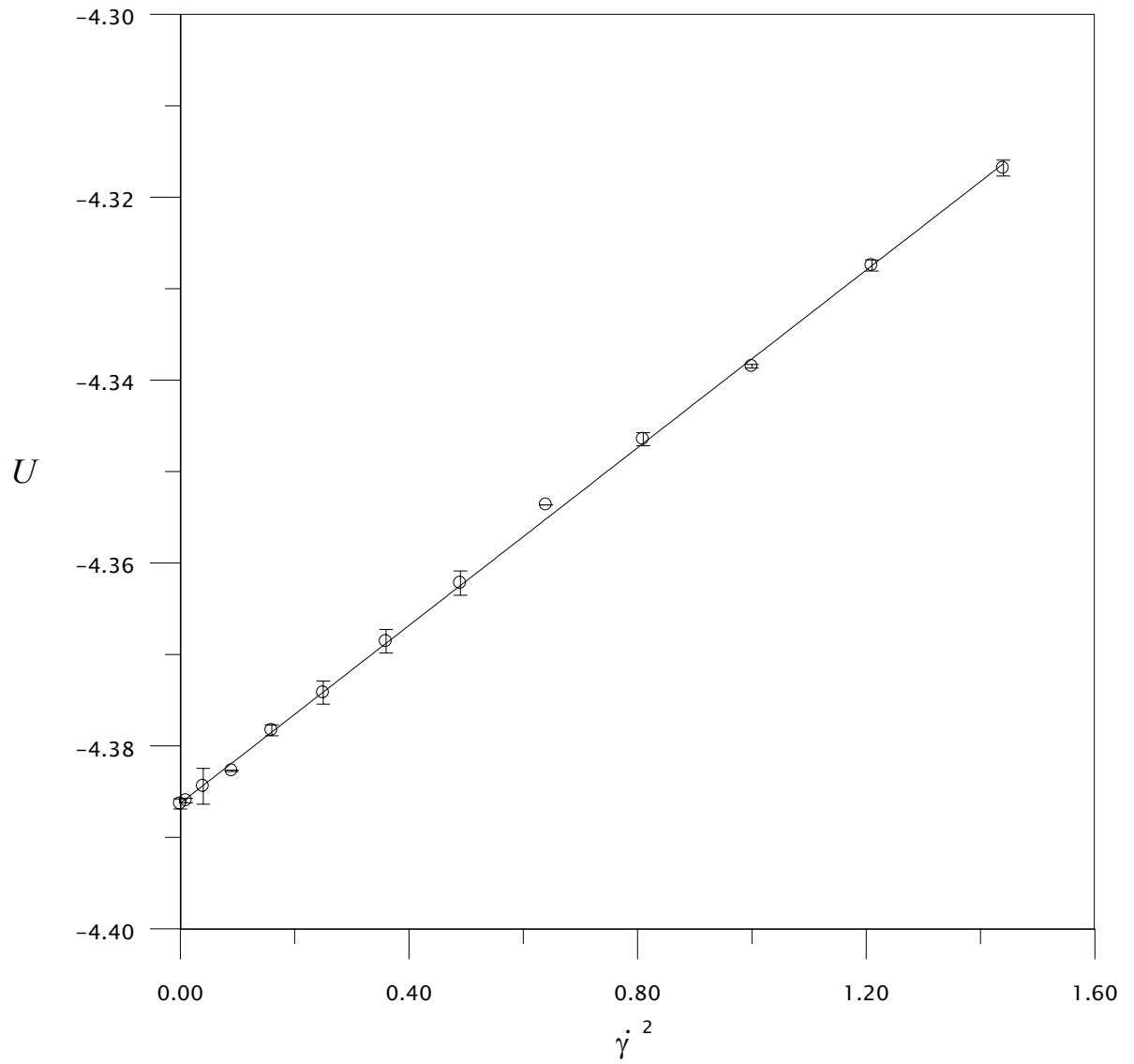


Figure 5.10 Potential energy per atom as a function of $\dot{\gamma}^2$ at high point.

The solid line shows a linear fit with an AAD of 0.01%.

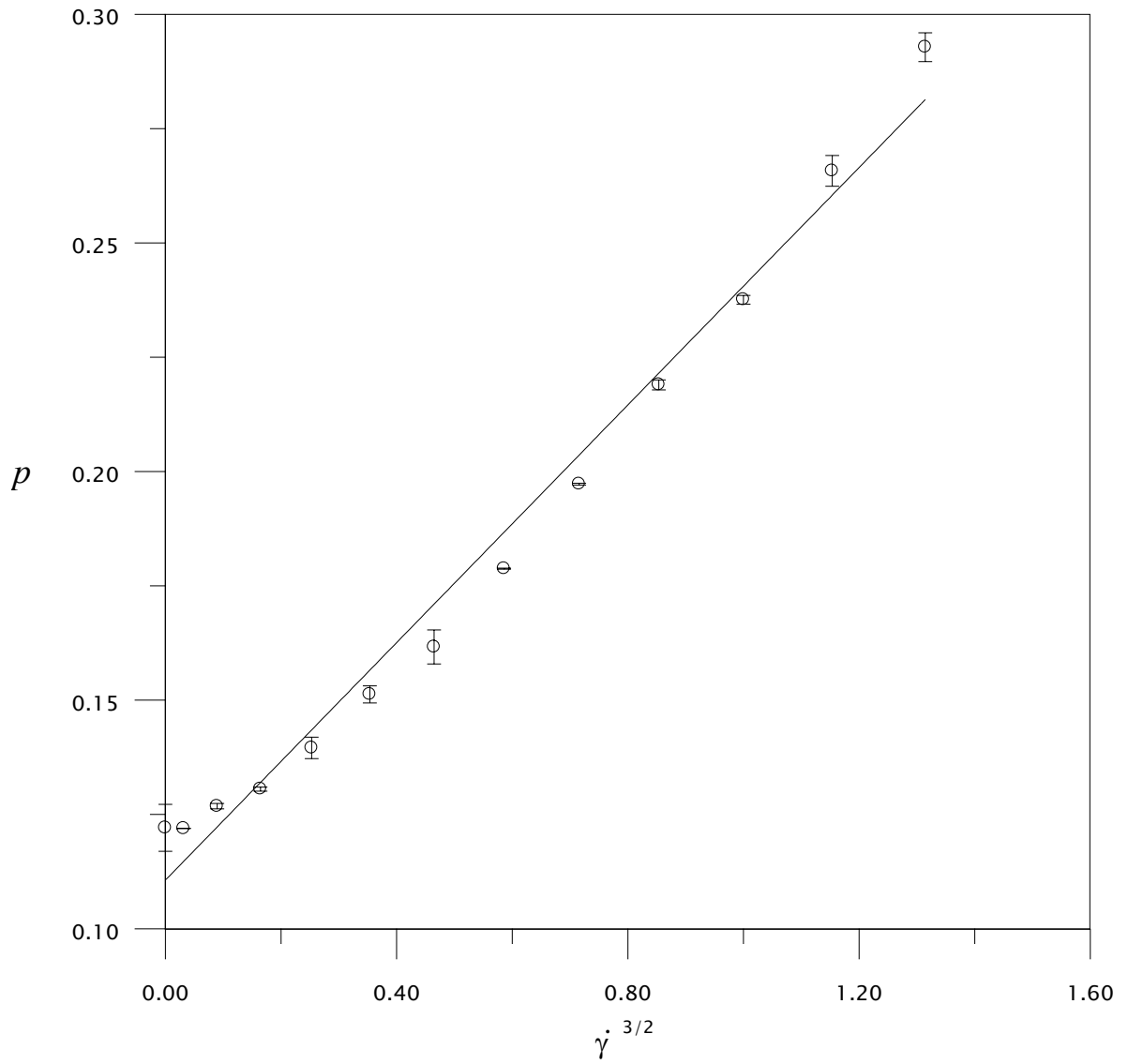


Figure 5.11 Pressure as a function of $\dot{\gamma}^{3/2}$ at high point.
The solid line shows a linear fit with an AAD of 0.84%.

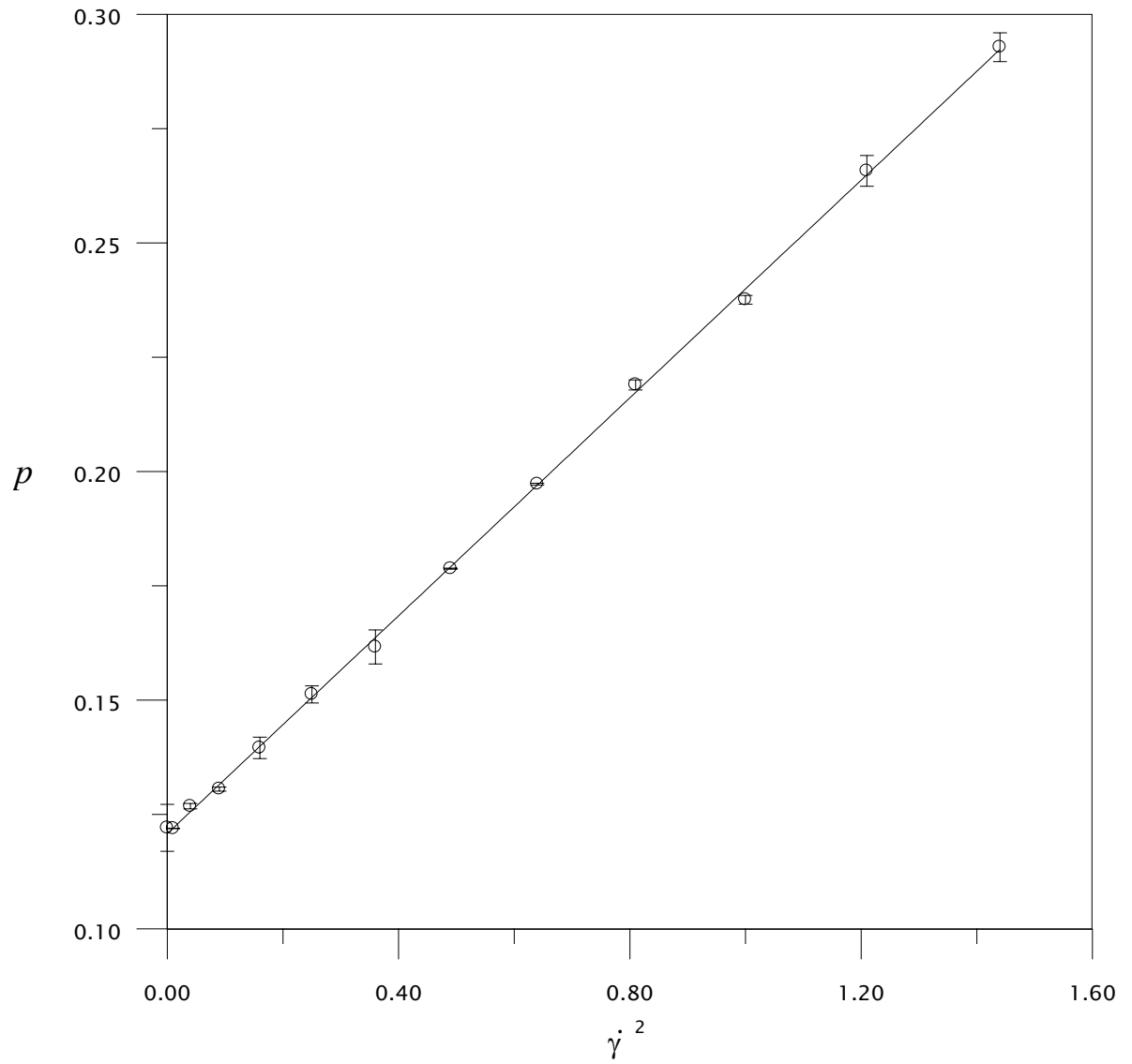


Figure 5.12 Pressure as a function of $\dot{\gamma}^2$ at high point.
The solid line shows a linear fit with an AAD of 0.19%.

5.3 Relationship between exponent and state point

In the section 5.2 we demonstrated by nonequilibrium molecular dynamics (NEMD) simulations that the accepted behaviour of simple fluids under planar shear flow, namely that the pressure and energy are linear functions of $\dot{\gamma}^{3/2}$, is only strictly true in the vicinity of the triple point. We showed that away from the triple point the behaviour of the exponent in the strain rate was closer to 2, suggesting a possible analytic dependence. In this section we explore this exponent dependence with greater precision and over a significant range of densities and temperatures, spanning the dense fluid region of the phase diagram for the Lennard-Jones fluid.

In our simulations we have ensured to explore only the dense fluid phase. Note here that ‘fluid’ in this strict sense may refer to liquid-vapour coexistence in some cases, but we have observed that this does not influence the shape of the strain rate profiles. We take care not to probe the liquid-solid coexistence region, as the strain rate profiles do not display simple power law behaviour in this region. The liquid-solid behaviour will be examined in detail in Chapter 6.

Our simulations are again performed on a Lennard-Jones 6-12 fluid of 500 atoms. We use a cut-off of $r_c = 3.5\sigma$, which is a value often cited in the literature by other workers. To characterize the phase diagram for this cut-off, we perform Gibbs ensemble calculations for the liquid-vapour coexistence curve [Pan87, Sad99]. The solid-liquid coexistence is taken from the literature [Kof93, Agr95], and the phase diagram is presented in Figure 5.13. All units quoted are reduced. Within the reduced temperature range of ~ 0.69 to 1.25 we may safely conduct simulations between reduced densities of ~ 0.7 to 0.84 and remain in the dense fluid region in the weak field limit.

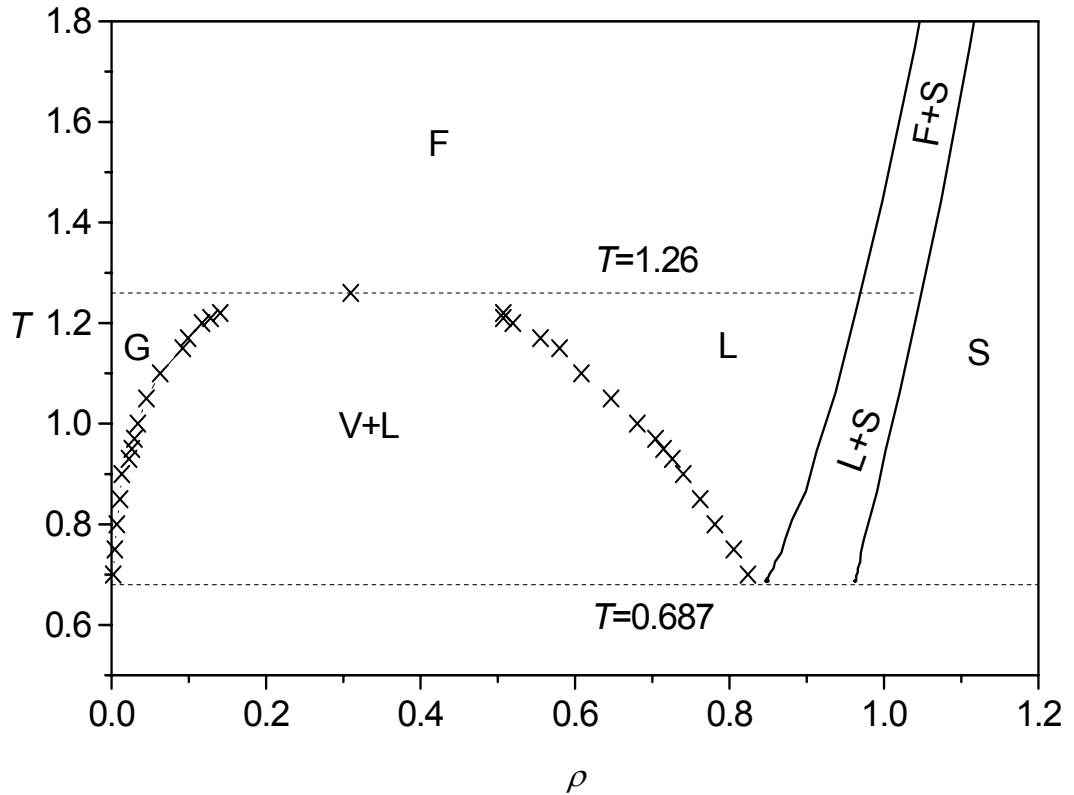


Figure 5.13 Phase diagram for the 6-12 Lennard-Jones fluid with a cut-off radius of $r_c = 3.5\sigma$. The triple point is located at $(\rho, T) = (0.85, 0.687)$, in agreement with ref [Kof93, Agr95], and the critical point is estimated as $(\rho, T) = (0.31, 1.26)$. The solid-liquid line is also obtained from [Agr95]. The vapour, liquid, fluid and solid phase regions are indicated by the symbols V, L, F and S, respectively.

Simulation run lengths varied according to the temperature/density requirements. For instance, simulations at low density (requiring long runs for good statistics) consisted typically of trajectories of 400000 τ , where $\tau = 0.001$ is the time step. Averages of all quantities are then taken over 30-40 trajectories of this length. For higher densities this could be reduced to ~ 10 trajectories of 200000 τ each while still preserving the same level of statistical accuracy. In all figures presented, error bars represent the standard error.

In what follows, we do not assume any value of the exponent in either the energy or pressure (e.g. 3/2 or 2), but determine its value *a-priori* via a least-squares fit of the quantity (energy or pressure) as a function of strain rate. We assume only that the total energy and pressure observe a power-law dependence of the form:

$$\begin{aligned} E &= E_0 + a\dot{\gamma}^\alpha \\ p &= p_0 + b\dot{\gamma}^\alpha \end{aligned} \tag{5.19}$$

where E_0 and p_0 are the total internal energy and pressure at equilibrium, and a and b are constants that depend on the density and temperature. This is certainly justifiable based on our previous work and that of Matin *et al.* [Mat00], and we typically find $\chi^2 \sim 10^{-5}$ for the fits to the data presented here. We then extract the value of α for each (ρ, T) state point, where for each state point we probe the range $0 \leq \dot{\gamma} \leq 0.6$ in steps of 0.1 reduced strain rate units (see Figure 5.14). This range encompasses both the Newtonian and non-Newtonian regimes. For simple fluids, a single exponent seems to be able to accurately describe the scaling behaviour of the pressure and energy at any particular state-point, within the range of uncertainties in our simulation data. Within these uncertainties we were unable to observe different power-law behaviour for the Newtonian region within the strain rates $0 \leq \dot{\gamma} \leq 0.1$. This is not the case for more complex polymeric fluids, in which different scaling exponents can be found in the Newtonian and non-Newtonian regimes (see for example ref. [Kro93]). Even if greater resolution was able to differentiate between different energy/pressure scaling parameters for the Newtonian and non-Newtonian regions in a simple fluid, our results are still valid in the non-Newtonian regime of relatively high strain rates.

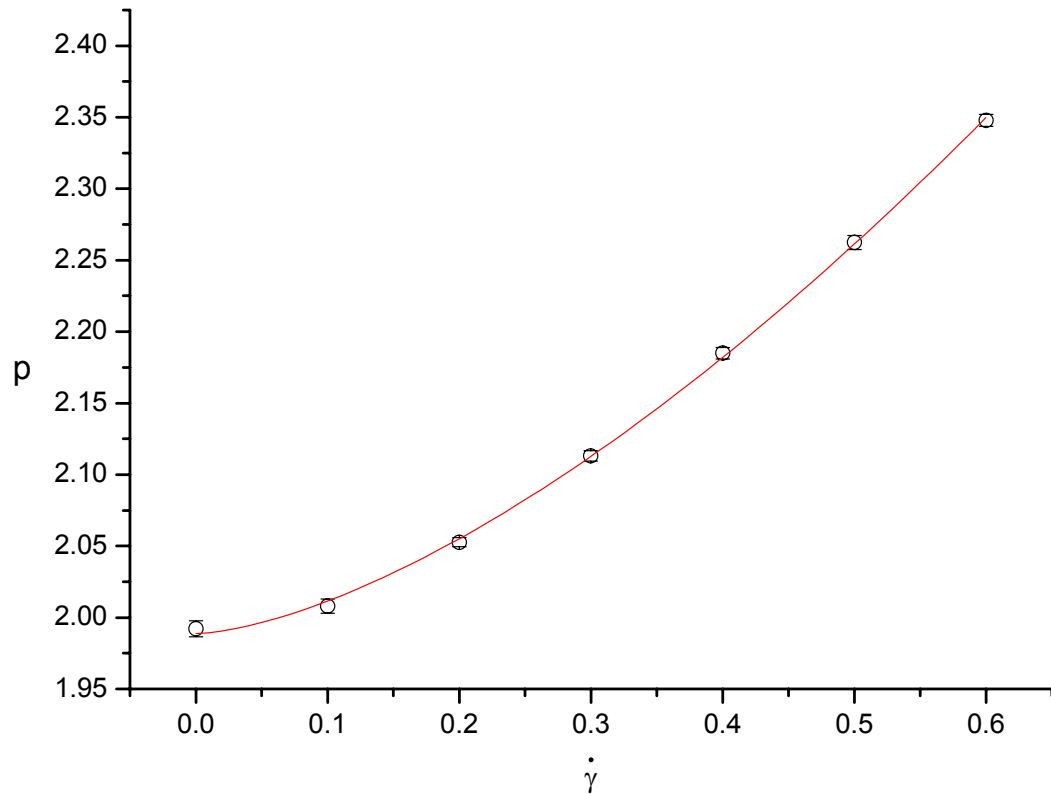


Figure 5.14 Pressure vs. strain rate at $T=1.0$, $\rho=0.8442$.

In Figure 5.15 we plot the exponent α computed for both the total potential energy per atom (U) and pressure (p) as a function of density for three different temperatures. Here U is defined as $U = \frac{1}{2} \sum_{i,j}^N u_{ij} / N$, where u_{ij} is the interatomic potential energy between atoms i and j , and N is the total number of atoms in the simulation. The pressure is calculated as $p = \frac{1}{3} \text{Tr}(\mathbf{P})$, where \mathbf{P} is the pressure tensor. We use potential energy to determine α (rather than total energy) as the temperature is constrained to a constant value and thus does not contribute to the shape of the energy vs. strain rate profile. The temperatures used span the entire range of possible values wherein the fluid will remain in the dense fluid region over the range of densities studied. There are three significant features to note: (i) at all temperatures, the exponent α is a linear function of density, maximum at low densities (~ 2),

decreasing continuously to a minimum at high densities (~ 1.2); (ii) the value of α is, within error bars, identical for both U and p , and (iii) the dense liquid phase is clearly non-analytic in strain rate. Further more, the widely accepted value of $\alpha = 3/2$ is only true in a very small region of the full available state-space, lying in a range of densities between (0.8, 0.9), depending on the temperature (increasing density with increasing temperature).

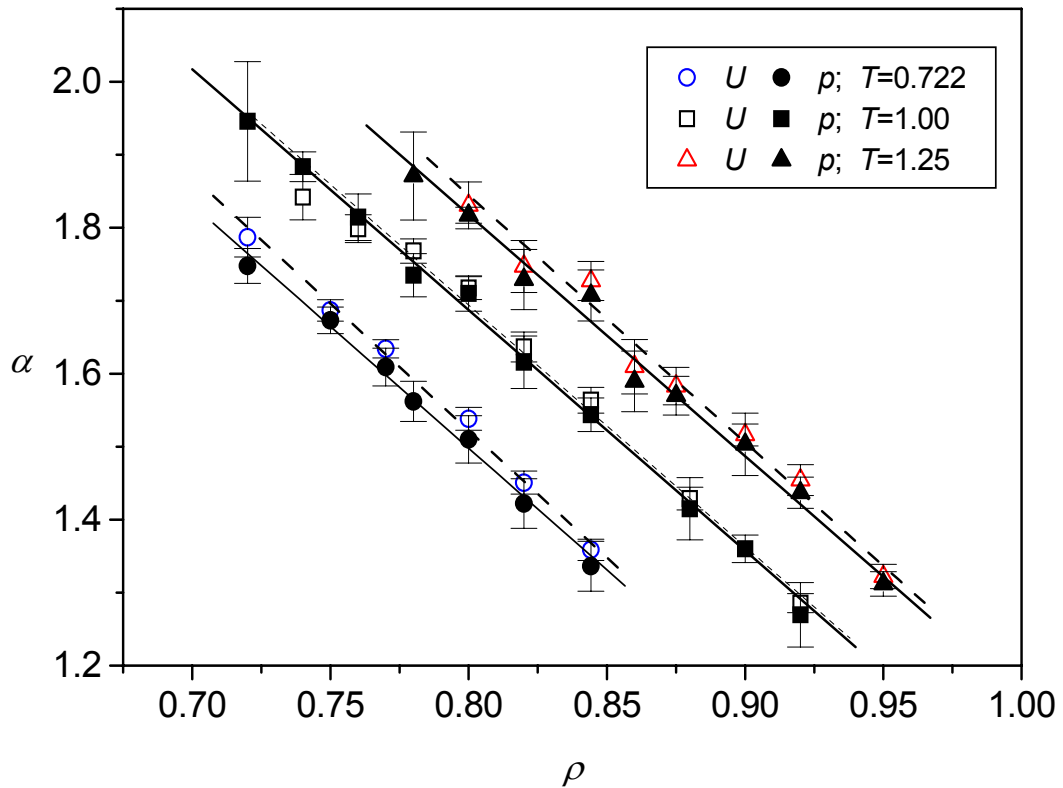


Figure 5.15 α as a function of density for different temperatures. All open symbols represent fits determined from the potential energy profile, whereas solid symbols refer to fits determined from the pressure profile.

In the expression (5.19), E_0 and p_0 are just the equilibrium energy and pressure. The other coefficients, a and b , are plotted in Figures 5.16 and 5.17.

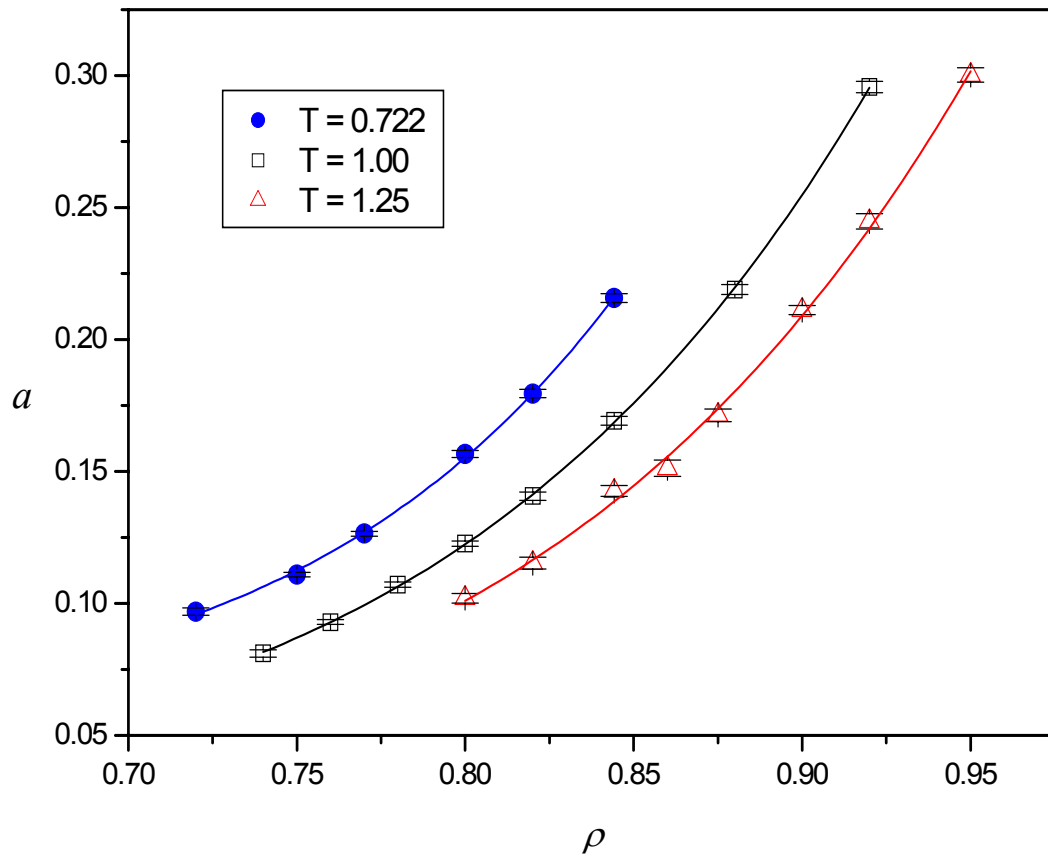


Figure 5.16 Coefficient a for energy at different temperatures.

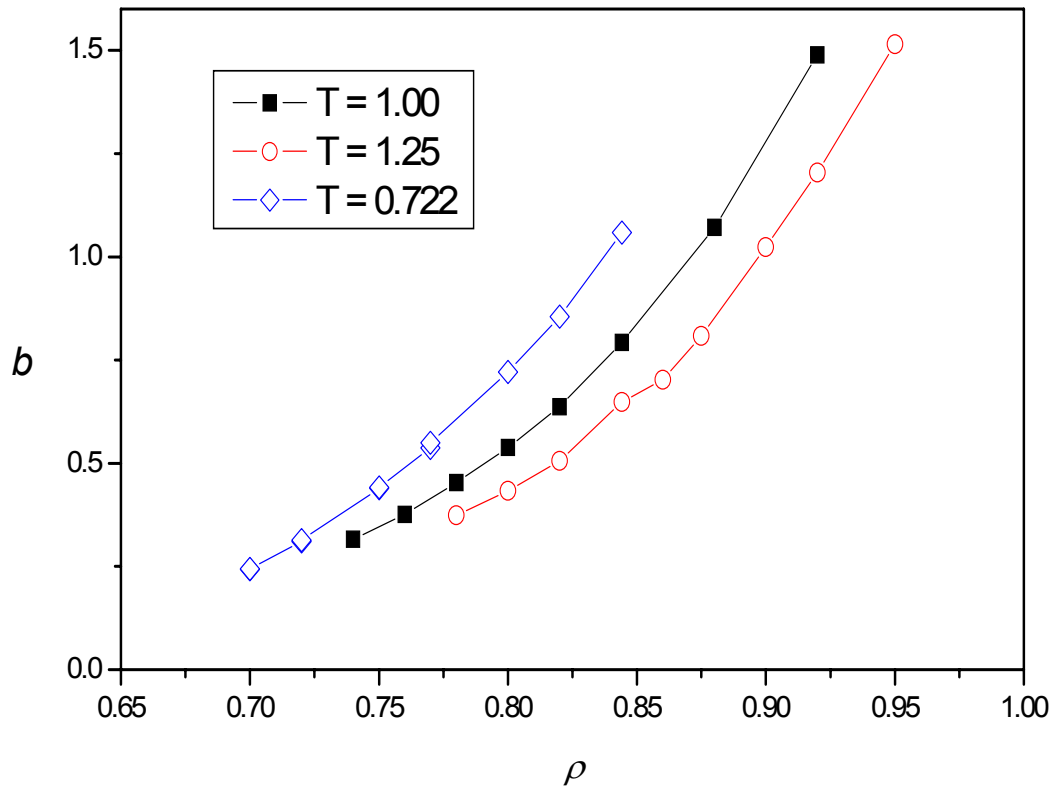


Figure 5.17 Coefficient b for pressure at different temperatures.

Unlike the pressure and energy exponents, we are unable to get an accurate function to account for the coefficients a and b , and so we only present the data here. However, a second order polynomial provides a reasonable approximation for the behaviour of these coefficients on density.

For energy,

$$T=0.722, \quad a = 2.39103 - 6.72202\rho + 4.91002\rho^2;$$

$$T=1.00, \quad a = 2.1323 - 5.93232\rho + 4.27451\rho^2;$$

$$T=1.25, \quad a = 2.68391 - 7.05846\rho + 4.78915\rho^2 .$$

For pressure,

$$T=0.722, \quad b = 7.17922 - 22.76252\rho + 18.36678\rho^2 ;$$

$$T=1.00, \quad b = 12.54798 - 34.96286\rho + 24.92679\rho^2 ;$$

$$T=1.25, \quad b = 15.16842 - 40.02185\rho + 27.00022\rho^2 .$$

We will not consider these coefficients further in this thesis.

There is another significant feature to come out of this study. The exponent α can be expressed as a simple linear function of both temperature and density:

$$\alpha = A + BT - C\rho \tag{5.20}$$

where A , B and C are coefficients with the constant values $A = 3.67 \pm 0.04$, $B = 0.69 \pm 0.03$, $C = 3.35 \pm 0.03$. The values of A , B and C are either universally true for all single component simple fluids (e.g. 11/3, 2/3 and 10/3, respectively), or else must be functions only of intermolecular potential. The significance of such a simple relationship is that it may now be possible to predict the pressure, energy, etc, of at least simple non-equilibrium fluids as a function of strain rate at any arbitrary thermodynamic state point in the dense fluid phase. Eqn (5.20) acts in an analogous way as an equation of state would, and can be used to characterize the scaling exponent α .

We note here that we did not apply any long-range corrections to our pressure or energy calculations. This is in fact unnecessary, as the long-range correction would only shift the (p, U) values by a constant amount [All89]; the shapes of the profiles (from which the α are calculated) remain unchanged. However, to ensure that α is independent of the value of cut-off used, we performed simulations at a cut-off of half the simulation box length, $r_c = L/2$ at a fixed temperature of $T=1.0$ over a range of liquid densities. Note that r_c will be

different for each ρ studied. We compare the value of α calculated for this system with those of our fixed cut-off ($r_c = 3.5\sigma$) in Figure 5.18 and find perfect agreement.

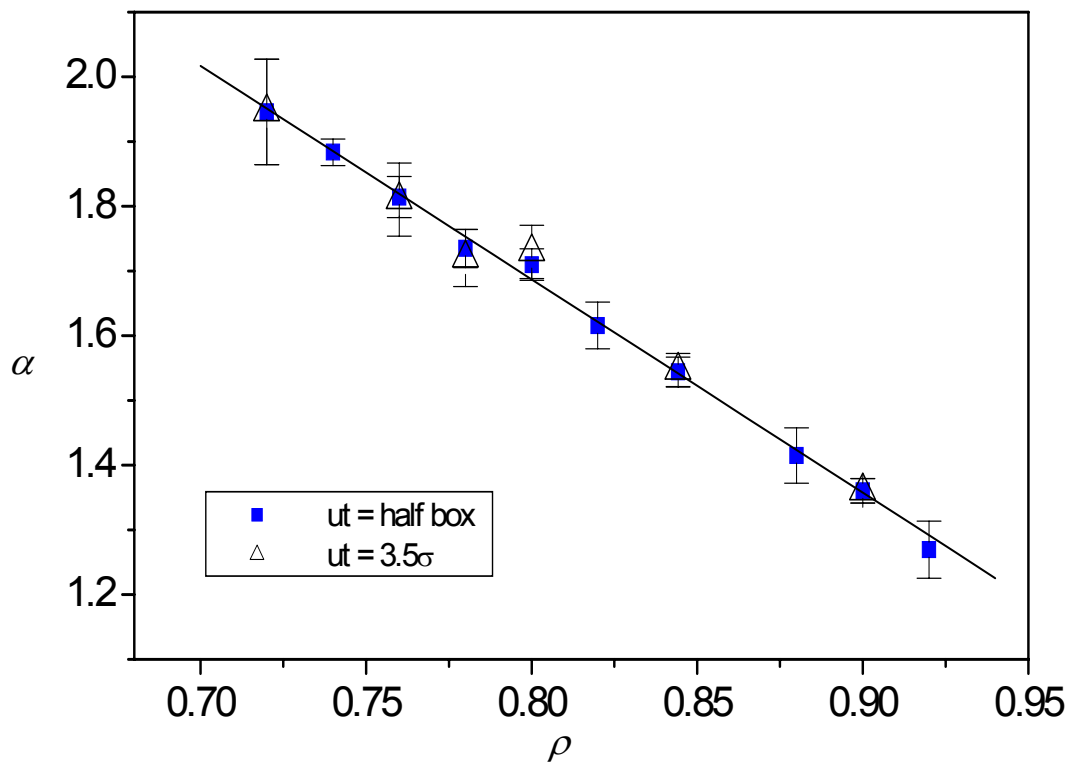


Figure 5.18 α as a function of density at $T = 1.0$ for cut-off $r_c = 3.5\sigma$ and $r_c = L/2$, where L is the simulation box length.

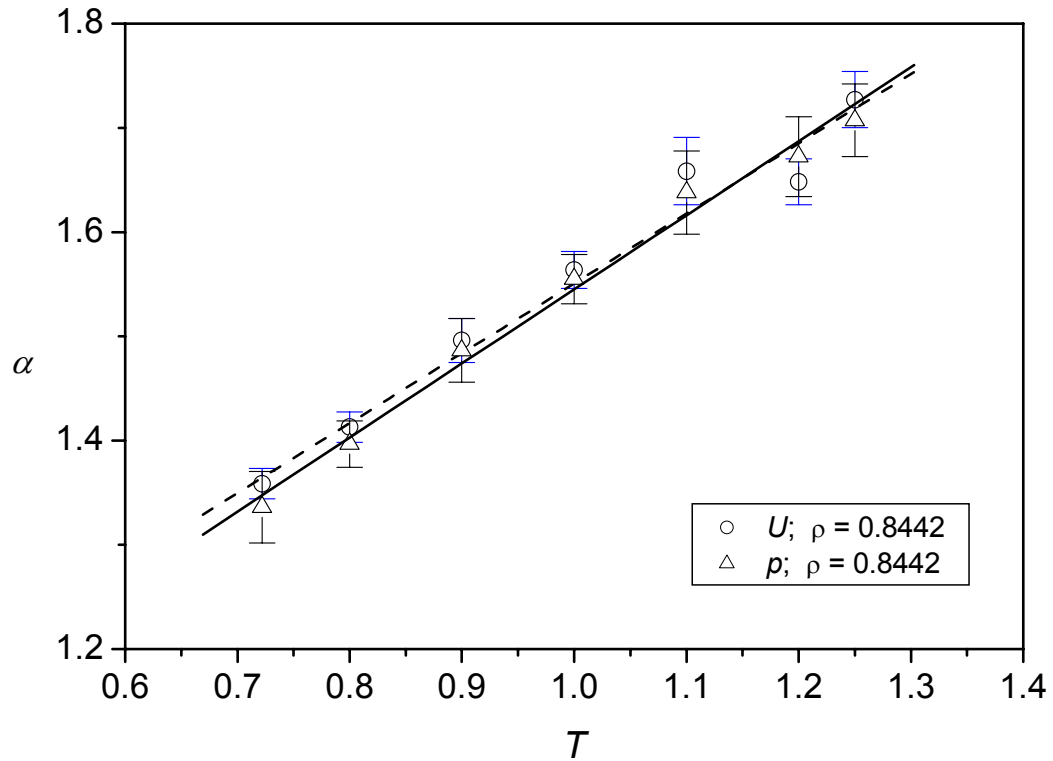


Figure 5.19 α as a function of temperature at $\rho = 0.8442$. Circles represent fits obtained from the potential energy profile, and triangles represent fits obtained from pressure profile.

In Figure 5.19 we plot α computed for both U and p as a function of temperature at a fixed density of 0.8442. As expected, the relationship is linear, but this time with a positive slope. Clearly, one could plot a three-dimensional curve in which α is displayed as a function of T and ρ , but as the curve would in fact be a plane in thermodynamic state-space there is no new insight to be gained by doing this.

Finally, to ensure that the fluid is non-analytic in strain rate, we also included the next allowable 4th order term in the pressure and energy Taylor series expansions (proportional

to $\dot{\gamma}^4$) (see section 5.1), but found that the fit can be extremely poor at state-points away from regions where $\alpha \sim 2$. Similarly, we tried fitting an exponential function to the data, with similarly poor results. We are thus confident that a simple power law relationship is valid within the strain rates studied in this work.

In Figure 5.20a we plot the shear viscosity vs. strain rate at the Lennard-Jones triple point. Figure 5.20b is the same plot, but on a logarithmic scale. These plots show the typical Newtonian and Non-Newtonian behaviour of the Lennard-Jones fluid, i.e. at relatively low strain rates the viscosity is constant (Newtonian) and decreases as a function of higher strain rates (Non-Newtonian).

We can presume that the relationship between viscosity and shear rate has the same power law form as pressure and energy, like Eqn. (5.19), but with different exponents:

$$\eta = \eta_0 + c\dot{\gamma}^\alpha \quad (5.21)$$

We can compute the exponent α in the same way as we computed the exponents for pressure and energy and show the results for two temperatures in Figure 5.21.

Because the viscosities obtained from our simulations have rather large error bars in the weak field region, especially at high temperature and low density, the exponents for viscosity obtained from the fitting are not accurate and it is difficult for us to confidently determine an accurate functional form to describe its behaviour. We note that the weak field simulations were performed using the transient time correlation function technique [Eva90], detailed in Chapters 4.8 and 8.

Despite this limitation, we can still see something significant from the state point dependence of viscosity. First, the exponent varies with state point. Increasing density or decreasing the temperature will induce a decreasing exponent. Second, if we use linear fitting for the data at two temperatures in Figure 5.21, their slopes are about -6.00 and -6.75 respectively. It is difficult for us to determine if the slopes are really parallel, as they are in

the case of energy and pressure (see Figure 5.15). Third, from the fitting results, we can see that the coefficient in Eqn. (5.21), c , is always negative and α is larger than zero, varying between ~ 0.1 to 2. From Eqn. (5.21), we know that the Lennard-Jones fluid is a shear-thinning fluid, though our simulations indicate that the degree of shear-thinning is a function of state point. Increasing density or decreasing temperature will reduce the degree of shear-thinning.

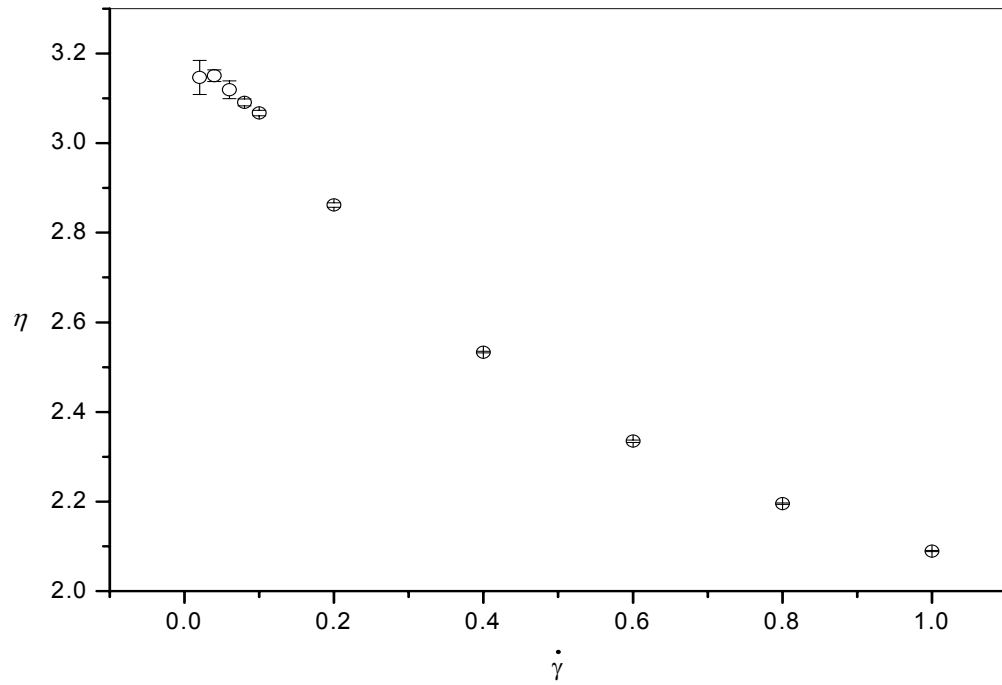


Figure 5.20a Viscosity vs. strain rate at the Lennard-Jones triple point.

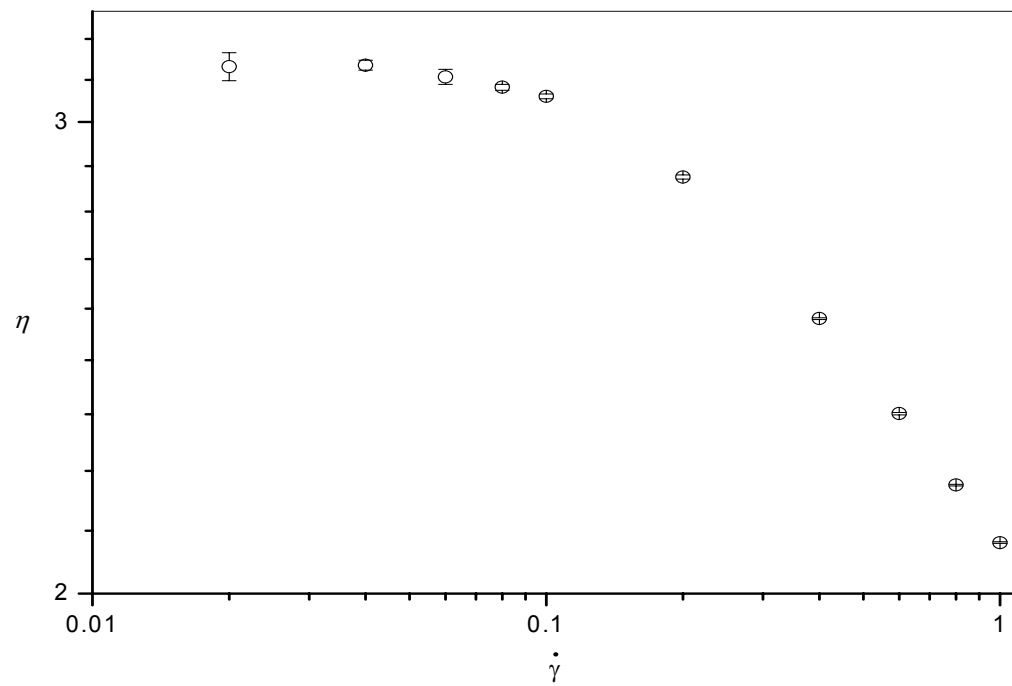


Figure 5.20b Same plot as Figure 5.20a, but on a logarithmic scale.

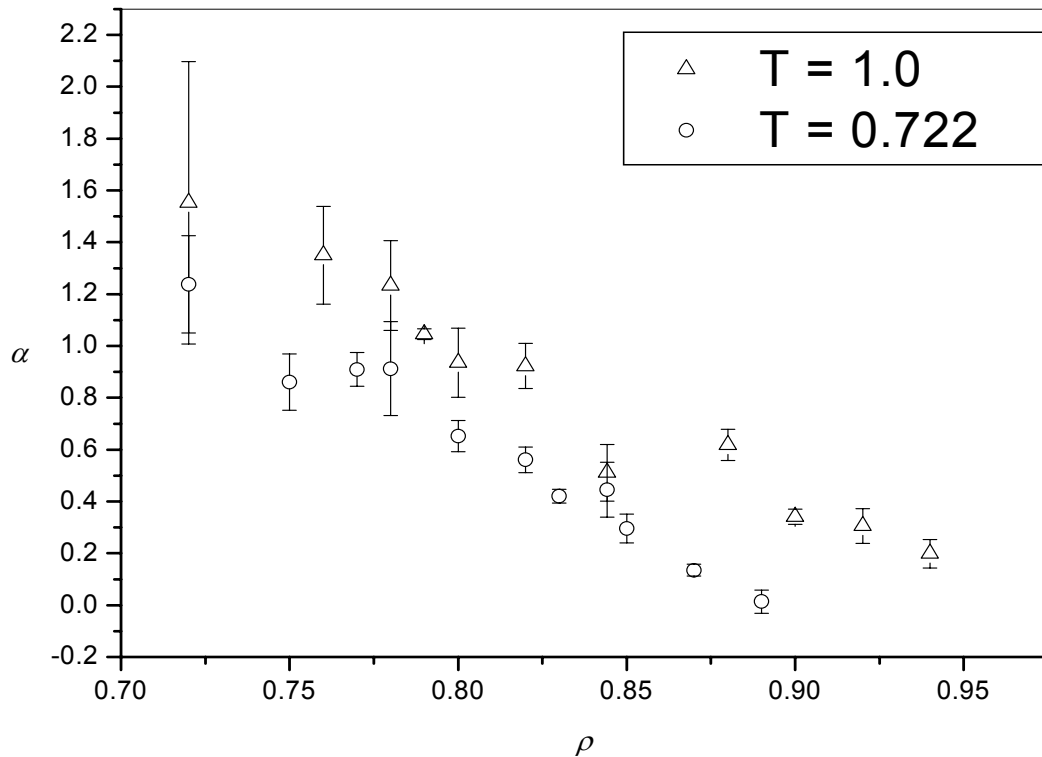


Figure 5.21 Exponent for the viscosity at two temperatures.

In conclusion for this chapter, we have for the first time characterized the strain rate exponent behaviour for the pressure, energy and viscosity of simple atomic Lennard-Jones fluids as a function of thermodynamic state point. We find that the fluid is non-analytic in strain rate for the range of strain rates studied here, but that the accepted $3/2$ and $1/2$ exponents have no special place in thermodynamic state-space, occurring in fact in a very limited region of relatively high density. A simple single linear relationship has been found that relates the exponent of both the pressure and energy strain rate profiles as a function of temperature and density. While it is likely that this linear relationship will be true for other intermolecular potentials (e.g., including those with 3-body interaction terms), an interesting question arises: are the values of the coefficients of equation (5.20) (A , B , C) independent of intermolecular potential, and hence “universal”, or functions thereof? In Chapter 7 we will consider this question further. It is hoped that our work will inspire other

liquid state theorists to re-examine the mode-coupling theory of Kawasaki and Gunton and either attempt to extend its validity into wider regions of thermodynamic state-space, or else devise a new theoretical framework to explain the observations reported here.